RESEARCH ARTICLE | MAY 18 2026

Flocking as a continuous phase transition in self-aligning active crystals

Marco Musacchio ; Alexander P. Antonov ; Hartmut Löwen ; Lorenzo Caprini

J. Chem. Phys. 164, 194903 (2026)
https://doi.org/10.1063/5.0332477

The Journal of Chemical Physics ARTICLE pubs.aip.org/aip/jcp

Flocking as a continuous phase transition in self-aligning active crystals

Cite as: J. Chem. Phys. 164, 194903 (2026); doi: 10.1063/5.0332477
Submitted: 4 March 2026 • Accepted: 1 May 2026 •
Published Online: 18 May 2026

Marco Musacchio,[1,a] Alexander P. Antonov,[1] Hartmut Löwen,[1] and Lorenzo Caprini[2,b]

AFFILIATIONS

[1] Institut für Theoretische Physik II: Weiche Materie, Heinrich-Heine-Universität Düsseldorf, Universitätsstraße 1, D-40225 Düsseldorf, Germany
[2] Physics Department, Sapienza University of Rome, Piazzale Aldo Moro 5, 00185 Rome, Italy

[a] Marco.Musacchio@hhu.de
[b] **Author to whom correspondence should be addressed:** lorenzo.caprini@uniroma1.it

ABSTRACT

We study a two-dimensional crystal composed of active units governed by self-alignment. This mechanism induces a torque that aligns a particle's orientation with its velocity and leads to a phase transition from a disordered to a flocking crystal. Here, we provide the first microscopic theory that analytically maps the crystal dynamics onto a Landau–Ginzburg model, in which the velocity-dependent effective free energy undergoes a transition from a single-well shape to a Mexican-hat profile. As confirmed by simulations, our theory quantitatively predicts the transition point and characteristic spatial velocity correlations. The continuous variation of the order parameter and the divergence of the analytically predicted correlation length imply that flocking in self-aligning active crystals corresponds to a continuous phase transition of the Berezinskii–Kosterlitz–Thouless type in two dimensions and to a second-order phase transition in three dimensions. These findings provide a theoretical foundation for the flocking phenomenon observed experimentally in active granular particles and migrating cells.

INTRODUCTION

Living systems across all length scales[1,2] display self-organization and collective phenomena, ranging from the flocking of animals to the swarming of bacteria[3] and the collective migration of cells.[4] Their natural behaviors have inspired the design of synthetic active matter units,[5] such as Quincke rollers[6,7] or active robots.[8–10] These systems often exhibit swarming or flocking phenomena[11–15] and have the potential to inspire innovative technologies.[16]

Over the last two decades, these perspectives have posed theoretical challenges in identifying the minimal ingredients required to reproduce these collective behaviors and in developing predictive theories. The observed collective movement is often modeled through explicit alignment interactions that couple the velocities of different particles.[17–23] This approach is inspired by the Ising and XY models,[24] originally introduced to describe the phase transition from paramagnetic to ferromagnetic materials. These velocity-aligning interactions have successfully described flocking in animals such as birds[25] and insects,[26] interpreting this phenomenon as a phase transition. In Vicsek-like models, flocking is explained through several theoretical approaches, ranging from Enskog-type kinetic theories[27–29] to hydrodynamic descriptions.[30–34]

In contrast to animals, active systems such as migrating cells and swarming robots are described by alternative aligning mechanisms. These systems are typically polar and are often characterized by a coupling between translational and rotational motion, commonly referred to as self-alignment.[35] This mechanism acts at the level of individual particles as an internal torque that tends to align the particle's orientation with its velocity. This torque differs from the one displayed in Vicsek-like models,[36–39] which, instead, couples the orientations of different particles. After being proposed to describe cells[40] and epithelial tissues,[41–44] self-alignment has been identified as the key mechanism governing the dynamics of polar active granular particles[45–47] self-propelling due to an internal motor[48–52] or a vibrating plate.[53–59] In these cases, self-alignment arises from a misalignment between the geometric center and the center of mass of the particle, generating a torque that aligns the

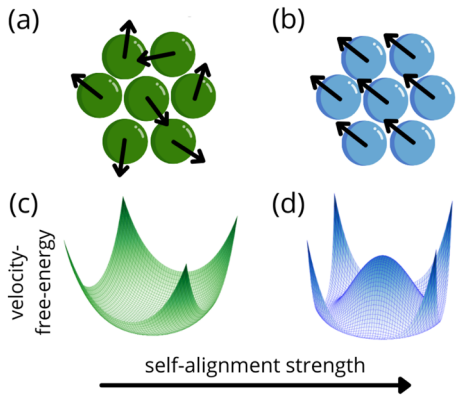

FIG. 1. Phase transition from a disordered to a flocking state in a self-aligning active crystal. Illustrations showing the disordered phase (a) and the flocking phase (b), where particle velocities are indicated by black arrows. (c) and (d) Corresponding Landau–Ginzburg velocity-free-energy profiles, transitioning from a single-well to a Mexican-hat-like profile.

particle's orientation with its velocity.

Self-alignment has been identified as the key mechanism inducing the flocking transition in polar granular systems,[60,61] as experimentally and numerically explored. At higher densities, such as self-aligning active liquids,[60,62–65] glasses,[66] and crystals,[67–70] the system undergoes a transition from a homogeneous disordered state to a homogeneous flocking one. These flocking phases emerge when the strength of the self-aligning torque dominates over the disruptive effects of translational and rotational noise.

However, despite systematic numerical investigations and its demonstrated relevance in experiments, a microscopic theory that fully captures the spontaneous collective motion induced by self-alignment is still lacking. Consequently, fundamental questions—such as whether the self-alignment-induced flocking transition is of first or second order—remain open.

We fill this gap by introducing, to the best of our knowledge, the first microscopic theory describing the flocking transition in dense self-aligning active matter. We map the dynamics of a self-aligning active crystal onto a Landau–Ginzburg model with a velocity-dependent free energy, which undergoes a phase transition from a single-well potential [Fig. 1(a)] corresponding to the disordered phase [Fig. 1(c)] to a Mexican-hat profile [Fig. 1(d)] corresponding to the flocking phase [Fig. 1(b)]. Consistently with our theory, the transition is of the Berezinskii–Kosterlitz–Thouless (BKT) type in two dimensions, while it is second order in three dimensions. The theory yields an exact prediction for the transition point as a function of self-alignment strength and persistence length and accurately captures both the spatial structure of velocity correlations and the associated correlation length.

RESULTS

Model for a self-aligning active crystal

We consider a two-dimensional system of N interacting active Brownian particles subject to a self-alignment mechanism. "Active" means that each particle moves persistently with a velocity aligned with its orientation, while "self-alignment" implies that this orientation tends to align with the particle's velocity due to a torque. Motivated by granular experiments, the particles can be described by inertial translational dynamics and overdamped rotational dynamics. The equations of motion for a particle with position $\mathbf{x}_i$, velocity $\mathbf{v}_i = \dot{\mathbf{x}}_i$, and orientational angle θ are given by

$$m\dot{\mathbf{v}}_i = -\gamma\mathbf{v}_i + \gamma v_0\hat{\mathbf{n}}_i + \mathbf{F}_i + \gamma\sqrt{2D_t}\,\boldsymbol{\xi}_i, \tag{1a}$$

$$\gamma_r\dot{\theta}_i = \mathbf{T}_i^{sa}\cdot\hat{\mathbf{e}}_z + \gamma_r\sqrt{2D_r}\eta_i. \tag{1b}$$

The terms γ and γ_r denote the translational and rotational friction coefficients, respectively, while D_t and D_r are the corresponding diffusion coefficients. The variables $\boldsymbol{\xi}_i$ and η_i represent the independent Gaussian white noises with zero mean and unit variance. Each particle, of mass m, is propelled at constant speed v_0 along the direction $\hat{\mathbf{n}}_i = (\cos\theta_i, \sin\theta_i)$, described by the orientational angle θ_i. This is subject to a deterministic torque $\mathbf{T}_i^{sa} = \beta\,(\hat{\mathbf{n}}_i \times \mathbf{v}_i)$, which aligns $\mathbf{n}_i$ to $\mathbf{v}_i$. The strength of the self-alignment is controlled by the parameter β, which sets the typical distance γ_r/β traveled by an active particle before its orientation aligns with its velocity. Finally, the force $\mathbf{F}_i$ models the pure repulsive interactions between the particles and is derived from a repulsive Weeks–Chandler–Andersen potential, $\mathbf{F}_i = -\nabla_i U_{tot}$, with $U_{tot} = \sum_{i<j} U(|\mathbf{r}_i - \mathbf{r}_j|)$ and $U(r) = 4\epsilon[(\sigma/r)^{12} - (\sigma/r)^6] + \epsilon$ for $r < \sigma 2^{1/6}$, and $U(r) = 0$ for $r \geq \sigma 2^{1/6}$. Here, ϵ sets the energy scale and σ represents the particle diameter. In our simulations, we set $D_t = 0$, since in active matter this term is typically lower than the effective diffusion induced by activity.

Self-alignment introduces an additional typical time, $\gamma_r/(\beta v_0)$, i.e., the time needed by the orientation to align with the velocity. This time competes with the other typical times governing the dynamics, i.e., the particle persistence time, $\tau = 1/D_r$, and the translational inertial time, $\tau_d = m/\gamma$. Simulations are performed by rescaling lengths by the particle diameter σ and time by τ. In this way, the dynamics are governed by several dimensionless parameters: the Péclet number $\mathrm{Pe} = v_0/(D_r\sigma)$, which quantifies the persistence length of the particle compared to its size; the reduced self-alignment strength $B = \beta\sigma/\gamma_r$, which compares the self-aligning length with the particle size; the reduced interaction strength, given by $\sqrt{\epsilon/m}/(D_r\sigma)$; and, finally, the reduced mass $M = D_r m/\gamma$, setting the relevance of inertia. We choose $M = 10^{-3}$ to effectively consider an almost overdamped limit so that inertia plays a negligible role. With this choice, we can avoid considering displacement vectors as velocities, since the vectors $\mathbf{v}_i$ are well-defined in the dynamics (1).

We focus on an active crystal composed of self-aligning active Brownian particles. Simulations of Eq. (1b) are performed in a two-dimensional square box of size L with periodic boundary conditions. A homogeneous crystalline configuration is obtained by setting a high packing fraction, $\Phi = N\sigma^2\pi/(4L^2) = 1.1$, which is consistent with a two-dimensional solid exhibiting almost perfect hexagonal order when L is sufficiently large. As known in previous studies,[66] when the self-alignment strength β/γ_r is sufficiently large compared to the particle persistence length v_0/D_r [Fig. 2(a)], the system shows a transition from a disordered [Fig. 2(b)] to a flocking phase [Fig. 2(d)], passing through the transition point [Fig. 2(c)]. The

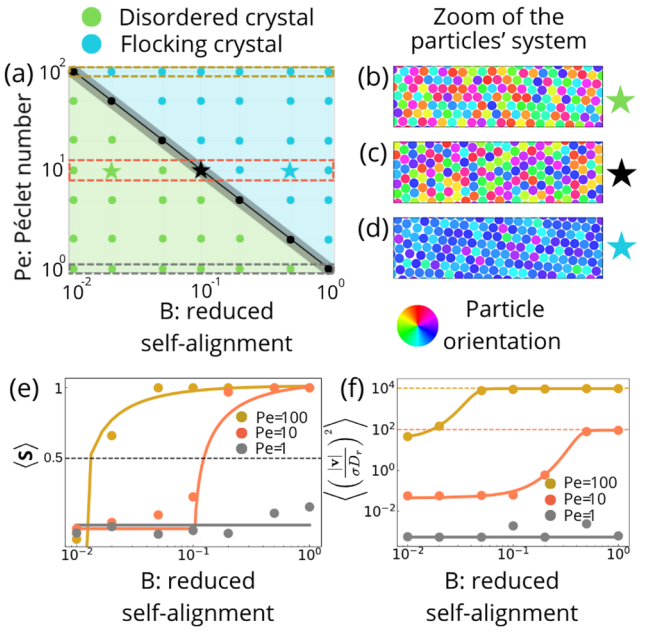

FIG. 2. Disordered-flocking phase diagram. (a) Phase diagram in the plane of the Péclet number $\mathrm{Pe} = v_0/(D_r\sigma)$ and the reduced self-alignment strength $B = \beta\sigma/\gamma_r$, showing disordered (green) and flocking (blue) crystals. (b)–(d) Rectangular zooms ($25\sigma \times 6\sigma$) of simulation snapshots corresponding to the three stars in the phase diagram. Particles' colors indicate the orientation of the particle. The black line marks the transition at $B \to B_c = \mathrm{Pe}^{-1}$ ($\beta_c/\gamma_r = 1/(v_0\tau)$), corresponding to the theoretical prediction (5), while the gray shaded area denotes the region where finite-size effects of the simulation hinder a clear identification of the system's phase. (e) Average polarization $\langle \mathbf{S} \rangle$ and (f) average squared velocity $\langle v^2 \rangle$ as functions of B for different Péclet numbers, in correspondence with the dashed rectangles in (a). The dashed black line in (e) marks 0.5, chosen as an indication for the transition from a disordered state ($\langle \mathbf{S} \rangle \sim 0$) to a flocking state ($\langle \mathbf{S} \rangle \sim 1$). Colored lines in (e) are obtained by plotting the theoretical prediction (6) with an additive constant accounting for finite size effects visible in the disordered phase. Colored, solid lines in (f) are guides for the eyes, while colored, dashed horizontal lines in (f) are drawn in correspondence with the free-particle speed—this is not reached for $\mathrm{Pe} = 1$. Numerical errors in (e) and (f) are smaller than the point size. The remaining dimensionless parameters of the simulations are $M = 10^{-4}$, $\sqrt{\epsilon/m}/(D_r\sigma) = 10^2$, and $\Phi = N\pi\sigma^2/4L^2 = 1.1$. The total simulation box is $L \times L$, where $L = 125\sigma$.

flocking transition is identified by monitoring the velocity polarization $\langle S \rangle = 1/N\langle |\sum_i \mathbf{v}_i/|\mathbf{v}_i|| \rangle$ [Fig. 2(e)] and the average squared velocity $\langle v^2 \rangle$ [Fig. 2(f)], as a function of the reduced self-alignment strength B. In a flocking configuration, $\langle S \rangle$ is close to the unit while $\langle v^2 \rangle$ approaches the single-particle velocity v_0. By contrast, in the disordered phase, $\langle S \rangle \ll 1$ while $\langle v^2 \rangle \ll v_0^2$. The flocking phase is also evidenced by the uniform color, indicating aligned particle orientations [Fig. 2(d)], whereas the disordered phase exhibits random orientations [Fig. 2(b)], a feature that persists at the critical point [Fig. 2(c)]. Indeed, for a quantitative characterization, we use the polarization to identify the flocking phase and its sharp transition, with $\langle S \rangle > 0.5$. Finally, we remark that the translational noise simply enhances random fluctuations. Therefore, when this term is larger than the self-propulsion force, thermal noise can suppress the flocking transition. Our choice of $D_t = 0$ helps us to highlight self-alignment-induced collective effects.

Theoretical mapping to a Landau–Ginzburg model

In this section, we report the main result of this paper: we derive a microscopic theory that predicts flocking in self-aligning active crystals. The theory analytically maps the dynamics (1) to a Landau–Ginzburg model, which allows us to conclude that the observed flocking phenomenon can be interpreted as a BKT transition in two dimensions, while it is second order in three dimensions.

By applying the time-derivative to the dynamics (1a) and eliminating $\dot{\mathbf{n}}_i$ using Eq. (1b), we can obtain an effective evolution equation for the particle velocity (see the section titled Methods), which is exact for $m/(\gamma\tau) \to 0$, i.e., the regime numerically evaluated. This theoretical mapping has already been applied in active systems without self-alignment,[71,72] for instance, to predict the wall accumulation typical of active Brownian particles.[73,74] In a crystal, we adopt the lattice approximation by assuming that particles occupy fixed positions on a lattice, such that the net force on each particle is balanced, $\mathbf{F}_i = 0$. Within this approximation that does not take into account phenomena such as particle dislocation and internal rearrangement of the system, the dynamics simplify (see the section titled Methods for details on the derivation) and are given by

$$\dot{\mathbf{v}}_i \approx -\sum_{j=1}^{n_i} \frac{\mathcal{K}}{\gamma}(\mathbf{v}_i - \mathbf{v}_j) + v_0\sqrt{\frac{2}{\tau}}\boldsymbol{\eta}_i - \mathbf{v}_i\left(\frac{1}{\tau} - \frac{\beta}{\gamma_r}v_0\right) - \frac{\beta}{\gamma_r v_0^2}\mathbf{v}_i|\mathbf{v}_i|^2, \tag{2}$$

where the sum $\sum_j^{n_i}$ is restricted to the six neighbors of the particle i, and $\boldsymbol{\eta}_i$ is a white noise vector with zero average and unit variance. The constant term $\mathcal{K}$ is related to the Hessian matrix of the interaction potential, i.e., its second derivative, and consequently, $\mathcal{K}$ mainly depends on the lattice structure (see the section titled Methods for details). In Eq. (2), the first line includes a noise contribution and an effective velocity-dependent interaction term $\mathcal{K}(\mathbf{v}_i - \mathbf{v}_j)$, which acts as a discrete Laplacian and promotes alignment of the velocities among neighboring particles. Compared to non-aligning active particles,[75,76] each $\mathbf{v}_i$ is additionally subject to a single-body, velocity-dependent force, as shown in the second line of Eq. (2).

To interpret the results, we switch from a particle-based description to a continuum approach for the velocity field $\mathbf{v}(\mathbf{r})$. This theoretical step is performed without introducing further approximations by simply replacing $\mathbf{v}_i \to \mathbf{v}(\mathbf{r})$ in the dynamics (2), obtaining the evolution for $\mathbf{v}(\mathbf{r})$,

$$\dot{\mathbf{v}}(\mathbf{r}) = -\frac{1}{\tau}\frac{\delta}{\delta\mathbf{v}(\mathbf{r})}\mathcal{F}[\mathbf{v}(\mathbf{r})] + v_0\sqrt{\frac{2}{\tau}}\boldsymbol{\eta}(\mathbf{r}), \tag{3}$$

where $\boldsymbol{\eta}(\mathbf{r}, t)$ is a white noise with zero average for every position $\mathbf{r}$, such that $\langle \boldsymbol{\eta}(\mathbf{r}, t)\boldsymbol{\eta}(\mathbf{r}', t') \rangle = \delta(t - t')\delta(r - r')$. This approximation for the noise term effectively replaces the active Brownian particle dynamics with its active Ornstein–Uhlenbeck counterpart. This method preserves the first and second moments of the stationary distribution, as verified in previous work,[77] and does not change

the polarization. The term $\mathcal{F} = \mathcal{F}[\mathbf{v}(\mathbf{r})]$ is an effective free-energy functional that uniquely depends on the velocity field,

$$\mathcal{F}[\mathbf{v}] = \int d\mathbf{r}\left[\tilde{\mathcal{K}}\nabla\mathbf{v}^2 + \left(1 - \frac{v_0\tau\beta}{\gamma_r}\right)\frac{|\mathbf{v}|^2}{2} + \frac{\tau\beta}{4\gamma_r}\frac{|\mathbf{v}|^4}{v_0^2}\right], \quad (4)$$

where $\tilde{\mathcal{K}} = \frac{3\tau\sigma^2\mathcal{K}}{2\gamma}$. This free energy has a Landau–Ginzburg shape and is characterized by the usual mass term $\propto \mathbf{v}^2$, interaction $\propto \mathbf{v}^4$, and gradient term $\propto (\nabla\mathbf{v})^2$ with coefficients depending on the persistence length $v_0\tau$ and self-alignment strength β. The gradient term favors the homogeneous phase, penalizing spatial changes of $\mathbf{v}(\mathbf{r})$, and is generated by the discrete Laplacian contribution proportional to $\propto \mathcal{K}$ in Eq. (2). By contrast, the mass and interaction terms are obtained by integrating over $\mathbf{v}$ the linear and cubic contributions in Eq. (2).

We remark that the mapping of the self-aligning active crystal dynamics onto a Landau–Ginzburg model for the velocity field $\mathbf{v}(\mathbf{r})$ is exact in the ideal crystal limit, where particle positions are frozen on lattice sites and the system exhibits crystal-like order. Consequently, our theoretical findings do not apply to self-aligning liquids or gases, which may also display density inhomogeneities, and cannot be used to predict the spectrum of the displacement field from the lattice positions. Nevertheless, our study establishes a connection between the physics of self-aligning active crystals and Landau–Ginzburg models in arbitrary spatial dimensions. This implies that the numerically observed transition from a homogeneous state to a flocking state corresponds to a BKT transition in two dimensions and to a second-order phase transition in three dimensions.

Prediction for the critical point and polarization

The sign of the mass term in the free-energy of the Landau–Ginzburg model determines the occurrence of a disordered or an ordered phase. When this term vanishes, the phase transition occurs. The mass term ($\propto \mathbf{v}^2$) in the effective free energy (4) changes sign when β exceeds the critical value β_c, given by

$$\frac{\beta_c}{\gamma_r} = \frac{1}{v_0\tau}, \quad (5)$$

corresponding to $B_c = \mathrm{Pe}^{-1}$. As a result, when the typical self-alignment length is larger than the persistence length, $\beta < \beta_c$ ($B < B_c$), the free energy is peaked at zero, implying the stability of the disordered phase. By contrast, in the opposite regime, $\beta > \beta_c$ ($B > B_c$), the free energy has a Mexican-hat shape, consistent with a flocking phase where rotational symmetry is broken. In this regime, the system displays a flocking behavior, characterized by a non-vanishing velocity field. The predicted transition point $\beta = \beta_c$ (or $B = B_c$) is consistent with our numerical findings [black line in Fig. 2(a)], taking into account that finite-size effects in the simulation hinder a clear identification of the system's phase around the transition line. To the best of our knowledge, this is the first theoretical microscopic prediction explaining the flocking behavior in self-aligning active systems.

From the expression (4), we can predict the polarization $\langle\mathbf{S}\rangle$ as a function of the self-alignment strength β (see the section titled Methods). In a disordered phase, $\langle\mathbf{S}\rangle \approx 0$ or reaches small values $\ll 1$ because of finite size effects [Fig. 2(e)]. By contrast, in the flocking state, $\langle\mathbf{S}\rangle$ can be estimated from the modulus of the velocity value, which minimizes the effective free-energy (4),

$$|\mathbf{S}| \approx \left(\frac{\gamma_r}{\beta}\right)^{1/2}\left(\frac{\beta}{\gamma_r} - \frac{1}{v_0\tau}\right)^{1/2} \propto \sqrt{\frac{B - B_c}{B}}. \quad (6)$$

As confirmed numerically, $\langle\mathbf{S}\rangle$ increases continuously with the square root of the reduced self-alignment strength B [Fig. 2(e)], displaying a behavior reminiscent of the magnetization curve in the Ising model.[24] This represents evidence that flocking in a self-aligning crystal undergoes a continuous phase transition.

Spatial velocity correlations and correlation length

Consistent with a Landau–Ginzburg model, the spatial velocity correlations $C(r) = \langle\sum_{ij}\mathbf{v}_i\cdot\mathbf{v}_j\delta(r - r_{ij})/\sum_{ij}\delta(r - r_{ij})\rangle$—with $r_{ij} = |\mathbf{r}_i - \mathbf{r}_j|$—have a spatial exponential shape $\sim e^{-r/\xi}/\sqrt{r}$ before the transition point [Fig. 3(a)]. Here, ξ corresponds to the correlation length of $C(r)$, which can be analytically predicted in the Gaussian approximation as

$$\xi = \frac{\sigma\sqrt{3\tau\mathcal{K}}}{\sqrt{\gamma}\left(1 - \frac{v_0\tau\beta}{\gamma_r}\right)^{1/2}} = \sigma\sqrt{\frac{3\tau\mathcal{K}}{\gamma}}\frac{1}{(1 - B\mathrm{Pe})^{1/2}}. \quad (7)$$

The correlation length ξ diverges at the transition point, occurring when $\beta/\gamma_r \to \beta_c = 1/(v_0\tau)$, i.e., when $B \to B_c = \mathrm{Pe}^{-1}$. This divergence is evident as ξ exceeds the system size [Fig. 3(b)], providing further confirmation that flocking in dense self-aligning systems undergoes a continuous phase transition. We also remark that the prediction (7) is consistent with previous results for active crystals in the absence of self-alignment ($\beta = 0$), as evidenced by the scaling with the persistence time $\xi \sim \sqrt{\tau\mathcal{K}}$.[78] For values of self-alignment bigger than the critical one, B_c, the correlation function $C(r)$ exhibits an almost flat profile, since each particle velocity is largely determined by the average value $\langle\mathbf{v}\rangle$ [Fig. 3(c)]. In two dimensions, this correlation decays algebraically, in agreement with the predictions of Landau–Ginzburg theory.[79–82] However, for parameter values far from the critical point, corresponding to sufficiently ordered systems, the decay of $C(r)$ is not observable within the accessible system sizes and would require simulations of larger systems.

By following Cavagna and Giardina,[83] we monitor the connected correlation function $C_c(r) = \langle\sum_{ij}\delta\mathbf{v}_i\cdot\delta\mathbf{v}_j\delta(r - r_{ij})/\sum_{ij}\delta(r - r_{ij})\rangle$—with $r_{ij} = |\mathbf{r}_i - \mathbf{r}_j|$, obtained by considering the deviation of the velocity field from its spatial average $\delta\mathbf{v}_i = \mathbf{v}_i - \langle\mathbf{v}\rangle$. This function $C_c(r)$ crosses zero and reaches negative values [Fig. 3(d)], as in previous studies on the flocking behaviors of birds.[83] Consistently, our system shows the typical scale-free properties of a flocking state: the curves for $C_c(r)$ collapse for different values of the parameters, being uniquely determined by the system size.

To confirm the nature of the phase transition predicted by our theory, we have numerically performed a finite-size scaling analysis in two dimensions. This study confirms the divergent behavior of the correlation length ξ as a function of the self-alignment strength, with a critical point B_c that is independent of the system size [Fig. 4(a)]. In Fig. 4, we show the self-alignment strength dependence of the polarization variance [Fig. 4(b)] and Binder cumulants [Fig. 4(c)]

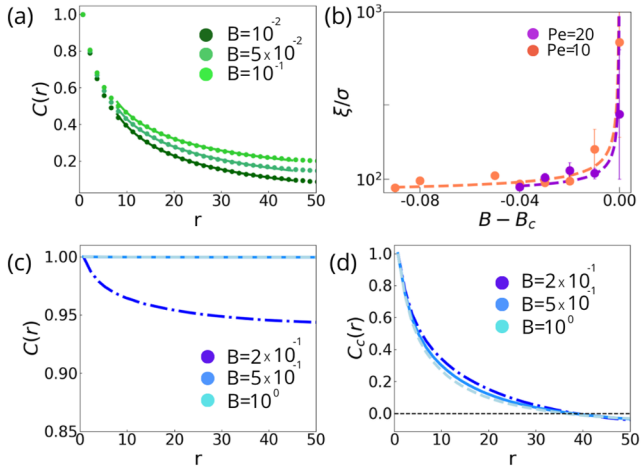

FIG. 3. Spatial velocity correlations and correlation length. (a) Spatial velocity correlations for different values of the reduced self-alignment strength B before the flocking transition at Pe = 10. The dashed lines represent the simulation data, while the solid curves correspond to the theoretical prediction, obtained by fitting the function $f(r) = a\, e^{-r/\xi}/\sqrt{r}$, where a and ξ are the fit parameters. (b) Correlation length ξ, obtained from the previous fits, is plotted as a function of $B - B_c$ for Pe = 20 and Pe = 10. Here, $B_c = \mathrm{Pe}^{-1}$ denotes the value of B at which the flocking transition occurs. The correlation length ξ exhibits a diverging behavior as the system approaches the critical point $\beta \to \beta_c = \gamma_r/(v_0\tau)$, corresponding to $B \to B_c = \mathrm{Pe}^{-1}$, in agreement with theoretical predictions. The critical points are marked with vertical dashed lines, shown in purple for Pe = 20 and in orange for Pe = 10 [Eq. (7)]. (c) and (d): Spatial velocity correlations $C(r)$ and connected spatial velocity correlations $C_c(r)$ after the flocking transition for different values of B at Pe = 10. The remaining dimensionless parameters of the simulations are $M = 10^{-4}$, $\sqrt{\epsilon/m}/(D_r\sigma) = 10^2$, and $\Phi = N\pi\sigma^2/4L^2 = 1.1$.

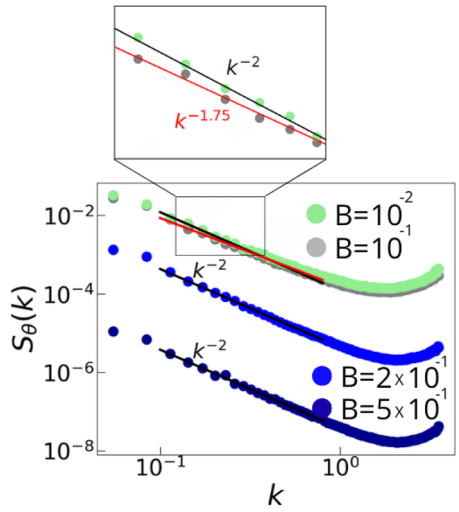

FIG. 5. Analysis of spectrum in Fourier space. Spectrum $S_\theta(k) = \langle \delta\hat{\theta}(k)\delta\hat{\theta}(-k)\rangle$ of the polar angle $\tilde{\theta}$ of the velocity as a function of the wave-vector k, where the tilde denotes the Fourier transform. $S_\theta(k)$ is shown for different values of self-alignment strength B and is compared with the scalings k^{-2} (black lines) and $k^{1/4-2} = k^{-1.75}$ (red line). The remaining dimensionless parameters of the simulations are Pe = 10, $M = 10^{-4}$, and $\sqrt{\epsilon/m}/(D_r\sigma) = 10^2$.

for various system sizes. All these results are consistent with a BKT transition rather than a first- or second-order transition, following Ref. 84: (i) the polarization variance exhibits no sharp peaks, showing only a smooth crossover near B_c, and does not change significantly with L, in contrast to a first-order transition where the peak grows as $\sim L^2$ or a second-order transition where the peak shifts around B_c; and (ii) the Binder cumulants merge to the value $U_L = 2/3$ in the ordered phase and show size dependence in the disordered phase, consistently with a BKT transition.[85] By contrast, a first-order transition exhibits a minimum in the Binder cumulant at B_c, while in a second-order transition, the cumulants cross at B_c, with $U_L(B_c) \to 2/3$ in the thermodynamic limit $L \to \infty$. Finally, the difference between a second-order and a BKT transition is more evident in the Fourier spectrum of the velocity polar angle correlation function, corresponding to the Goldstone mode for $B > B_c$ (Fig. 5). In our case, for the Goldstone mode, it follows the behavior $S_\theta(k) = \langle \delta\hat{\theta}(k)\delta\hat{\theta}(-k)\rangle \sim k^{-2}$, and for the transition point $B \sim B_c$, it yields the scaling $S_\theta(k) \sim k^{\eta-2}$, with the value $\eta = 1/4$ consistent with the BKT transition.[86] In the disordered phase $B < B_c$, it goes back to the $S_\theta(k) \sim k^{-2}$, in accordance with an Ornstein–Zernike

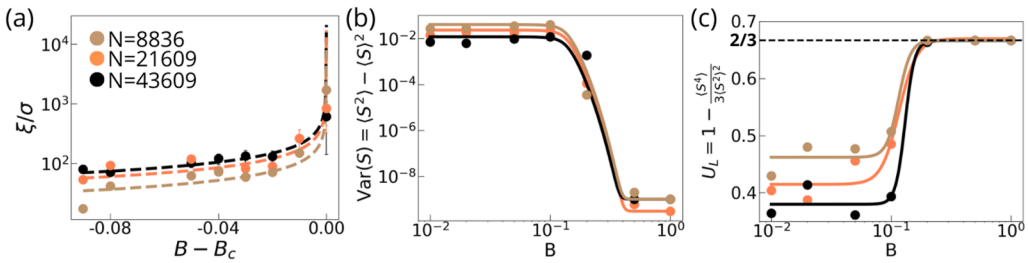

FIG. 4. Finite-size scaling analysis. (a) Correlation length ξ, normalized by the particle diameter σ, as a function of the reduced self-alignment strength $B - B_c$, where $B_c = \mathrm{Pe}^{-1}$ is the value of B at which the flocking transition occurs. (b) Polarization variance $\mathrm{Var}(\mathbf{S}) = \langle \mathbf{S}^2\rangle - \langle|\mathbf{S}|\rangle^2$ as a function of B. Here, the dashed line marks the value 2/3, at which U_L converges in the ordered phase. (c) Binder cumulant $U_L = 1 - \langle \mathbf{S}^4\rangle/(3\langle \mathbf{S}^2\rangle^2)$ as a function of B. Data are shown for different system particle numbers $N = 8836, 21\,609, 43\,609$, with the corresponding system lengths L chosen to keep the packing fraction fixed at $\Phi = 1.1$. The legend shown in panel (a) applies to panels (b) and (c). The remaining dimensionless parameters of the simulations are Pe = 10, $M = 10^{-4}$, and $\sqrt{\epsilon/m}/(D_r\sigma) = 10^2$.

profile.[87–90] It is, nevertheless, important to remark that our numerical study is consistent with the BKT scenario, but a clear identification of a BKT transition would require the analysis of topological defects and universal scaling properties, which is beyond the scope of the present work.

CONCLUSIONS

Our study provides one of the first microscopic theories for the flocking phenomenon in self-aligning active crystals by establishing a theoretical link between self-aligning active matter and the well-established Ginzburg–Landau model used to describe order–disorder phase transitions. The self-alignment strength induces a sign change in the mass term of the effective velocity-dependent free energy, giving rise to a symmetry breaking in the rotational symmetry of the system and, consequently, Goldstone modes. In contrast to Vicsek-like models,[91–93] our velocity-dependent Landau–Ginzburg theory predicts that flocking in self-aligning active crystals is a Berezinskii–Kosterlitz–Thouless (BKT) transition in two dimensions, as also suggested by the simulations' results, and a second-order phase transition in three dimensions. This is evidenced by the continuous change of the order parameter—the velocity polarization—and by the divergence of the correlation length of the spatial velocity correlations.

Compared to Vicsek-like models, flocking is observed here without an explicit coupling between different particle velocities. However, to achieve this global movement, both repulsive interactions and self-alignment are crucial, as evidenced by our theory: in the absence of self-alignment, the mass term never changes sign, and the disordered phase remains stable. Indeed, collective motion in crystals composed of non-aligning active Brownian particles cannot be observed,[89,94–97] except in the limit of infinite persistence length.[98] Consequently, although our microscopic theory is strictly valid in the ideal crystal limit, it could be extended to less dense regimes by relaxing the underlying assumptions. This may justify the formulation of a hydrodynamic description in self-aligning active matter and could inspire a more systematic theoretical study, for instance, through a Toner–Tu theory[30] to explore lower density configurations. In these cases, density inhomogeneities may develop in the form of bands or moving crystals,[65] features that are not observed in systems with underlying crystalline order.

This work thus offers a solid theoretical foundation for understanding collective behavior in high-density active granular matter exhibiting swarming or flocking, as well as in migrating biological systems, such as cell monolayers or living tissues, which are often modeled through self-alignment mechanisms. In particular, our predictions for the flocking transition point and the correlation length of the system can be quantitatively tested through granular HexBug particles linked by springs. Compared to this work, we expect that larger system sizes may be required to suppress finite-size effects and reach the predicted flocking transition point. We note, however, that our theory does not capture the collective displacement modes observed experimentally in Ref. 69. This limitation arises because our theoretical analysis is performed within a lattice approximation, in which particle positions are fixed on lattice sites and fluctuations in their displacements are not resolved. Indeed, it would be interesting to carry out a more systematic study as a function of density in self-aligning active systems. We expect that dislocations and disclinations occurring by lowering the density may influence the nature of the phase transition or change the transition point from a homogeneous to a flocking phase. It may also be worthwhile to investigate how the flocking transition is affected in the two-dimensional hexatic phase, as recent studies[99] on doping two-dimensional crystals with active particles have shown that melting in two dimensions is directly governed by defect concentration. Another direction that should be addressed in future studies is the identification of the universality class of this transition, as well as whether the continuous phase transition persists upon the introduction of quenched disorder into the system.[100–102]

Beyond active granular matter, our theory may also apply to other systems that exhibit flocking-like behavior[103,104] or collective migration. This includes biological cells, which are often modeled using self-alignment interactions,[4] as in our approach. Moreover, the theoretical framework we propose can be extended to systems dominated by anti-self-alignment, in which particle orientations tend to align antiparallel to their velocities. Such mechanisms have been invoked not only in active granular systems[61] but also recently to describe human crowds.[105] Incorporating this anti-alignment term into our theory—holding in a solid-like regime—may enable predictions of the collective chiral oscillations observed experimentally.

METHODS

Details on the numerical simulations

The dynamics described in the main text by Eqs. (1a) and (1b) are numerically implemented by using the Euler integration scheme with a time step of $\Delta t = 5 \times 10^{-6}\tau$. Rescaling time by the persistence time of the particle's trajectory, τ, and positions by the particle's diameter, σ, the integration scheme is as follows:

$$\mathbf{r}_i'(t' + \Delta t') = \mathbf{r}_i'(t') + \Delta t' \mathbf{v}_i'(t'), \tag{8a}$$

$$\mathbf{v}_i'(t' + \Delta t') = \mathbf{v}_i'(t') - \frac{\gamma}{mD_r}\Delta t' \gamma \mathbf{v}_i'(t') + \Delta t' \frac{1}{\sigma m D_r^2}\mathbf{F}'_i(\mathbf{r}_i'(t')) + \frac{\gamma}{mD_r}\Delta t' v_0' \hat{\mathbf{n}}_i, \tag{8b}$$

$$\theta_i'(t' + \Delta t') = \frac{\beta\sigma}{\gamma_r}\Delta t' (\hat{\mathbf{n}}_i \times \mathbf{v}_i') \cdot \hat{\mathbf{e}}_z + \sqrt{2\Delta t'} Y_i. \tag{8c}$$

In the equations presented, the prime symbol denotes the dimensionless variables used in our simulations. In this formulation, the orientation is given by $\hat{\mathbf{n}}_i = (\cos\theta_i, \sin\theta_i)$, while Y_i are the Gaussian random variables with zero mean and unit variance. The force due to a potential can be expressed as $\mathbf{F}_i = -\nabla_i U_{tot}$, with $U_{tot} = \sum_{i<j} U(|\mathbf{x}_i - \mathbf{x}_j|)$, where U is chosen as a WCA potential, as explained in the main text. The particle dynamics are governed by several dimensionless parameters, introduced in the main text: the Péclet number, $\mathrm{Pe} = v_0/(D_r\sigma)$, which quantifies the activity strength and is varied from Pe = 1 to Pe = 100 in the numerical study; the reduced mass, $M = D_r m/\gamma$, which compares the inertial time m/γ with the persistence time $\tau = 1/D_r$ and corresponds to the inverse of the coefficient multiplying the second and last terms on the right-hand

side of Eq. (8b). This is fixed to $M = 10^{-4}$ so that a low inertia regime is explored and the dimensionless interaction strength, $\sqrt{\epsilon/m}/(D_r\sigma)$, can be extracted by manipulating the third term of the same equation. Self-alignment introduces an additional dimensionless parameter, i.e., the reduced self-alignment strength, $B = \beta\sigma/\gamma_r$, which is varied in the range $10^{-2} \leq B \leq 10^{0}$. Simulations are performed for a total time of $2 \times 10^2\tau$ in a square box of size $L = 125$ with $N = 2.2 \times 10^4$ particles, yielding a packing fraction of $\Phi = N\pi\sigma^2/4L^2 = 1.1$.

Derivation of the theoretical results

Algebraic manipulation of the self-aligning active dynamics

The dynamics for two-dimensional active Brownian particles [Eq. (1)], interacting with self-alignment or anti-self-alignment mechanisms, can be expressed in Cartesian components as follows:

$$\dot{\mathbf{v}}_i = \frac{\mathbf{F}_i}{m} - \frac{\gamma}{m}\mathbf{v}_i + \frac{\gamma}{m}v_0\hat{\mathbf{n}}_i, \tag{9a}$$

$$\dot{\hat{\mathbf{n}}}_i = -\frac{\hat{\mathbf{n}}_i}{\tau} + \sqrt{\frac{2}{\tau}}\boldsymbol{\eta}_i \times \hat{\mathbf{n}}_i + \frac{\beta}{\gamma_r}(\hat{\mathbf{n}}_i \times \mathbf{v}_i) \times \hat{\mathbf{n}}_i, \tag{9b}$$

where $\mathbf{v}_i = \dot{\mathbf{x}}_i$ and we have introduced the white noise vector with components $\boldsymbol{\eta}_i = (0, 0, \eta_i)$. The resulting stochastic noise, proportional to $\boldsymbol{\eta}_i \times \hat{\mathbf{n}}_i$, is multiplicative and is interpreted in the Itô sense. We emphasize that the term $-\hat{\mathbf{n}}_i/\tau$ arises from adopting the Itô convention for stochastic integration upon transforming the angular dynamics from polar to Cartesian coordinates.[106] Finally, in the dynamics (9a), we have neglected the translational noise, which is usually irrelevant in active matter systems.

As a first step, we note that the self-alignment interactions can be expressed in the following form:

$$\beta(\hat{\mathbf{n}}_i \times \mathbf{v}_i) \times \hat{\mathbf{n}}_i = \beta(\mathbf{v}_i - \hat{\mathbf{n}}_i[\mathbf{v}_i \cdot \hat{\mathbf{n}}_i]), \tag{10}$$

where we have used that $\mathbf{n}_i$ is a unit vector such that $\mathbf{n}_i^2 = 1$. At first, we define the acceleration $\mathbf{s}_i = \dot{\mathbf{v}}_i$ and then apply the time derivative to Eq. (9a). By using Eq. (9b) to calculate $\dot{\hat{\mathbf{n}}}_i$, we obtain

$$\dot{\mathbf{s}}_i = -\frac{\gamma}{m}\mathbf{s}_i - \mathbf{v}_j \cdot \nabla_i\nabla_j\frac{U_{tot}}{m} + \frac{\gamma v_0}{m}\left[-\frac{\hat{\mathbf{n}}_i}{\tau} + \sqrt{\frac{2}{\tau}}\boldsymbol{\eta}_i \times \hat{\mathbf{n}}_i + \frac{\beta}{\gamma_r}(\mathbf{v}_i - \hat{\mathbf{n}}_i[\mathbf{v}_i \cdot \hat{\mathbf{n}}_i])\right]. \tag{11}$$

Finally, by using Eq. (9a), we eliminate $\mathbf{n}_i$ in favor of $\mathbf{s}_i$, $\mathbf{v}_i$, and the force $\mathbf{F}_i$ so that the dynamics are expressed as a function of position, velocity, and acceleration only, as

$$\dot{\mathbf{s}}_i = -\left(\frac{\gamma}{m} + \frac{1}{\tau}\right)\mathbf{s}_i - \mathbf{v}_j \cdot \nabla_i\nabla_j\frac{U_{tot}}{m} + \frac{\mathbf{F}_i}{m\tau} + \frac{\gamma v_0}{m}\sqrt{\frac{2}{\tau}}\boldsymbol{\eta}_i \times \hat{\mathbf{n}}_i + \frac{\gamma}{m}\mathbf{v}_i\left(-\frac{1}{\tau} + v_0\frac{\beta}{\gamma_r}\right) - \frac{\gamma v_0}{m}\frac{\beta}{\gamma_r}\left[\left(\frac{m}{\gamma v_0}\mathbf{s}_i + \frac{\mathbf{v}_i}{v_0} - \frac{\mathbf{F}_i}{\gamma v_0}\right)\mathbf{v}_i \cdot \left(\frac{m}{\gamma v_0}\mathbf{s}_i + \frac{\mathbf{v}_i}{v_0} - \frac{\mathbf{F}_i}{\gamma v_0}\right)\right]. \tag{12}$$

The dynamics (12) are equivalent to the equations of motion (9a) and (9b) numerically implemented and result from a change of variables from $(\mathbf{x}_i, \mathbf{v}_i, \hat{\mathbf{n}}_i)$ to $(\mathbf{x}_i, \mathbf{v}_i, \mathbf{s}_i)$.

Vanishing inertia limit

By considering the limit of small inertia, one can select the leading contributions to the dynamics (12) in the limit of small m/γ. In particular, we consider terms proportional to γ/m and neglect higher-order contributions, obtaining

$$\dot{\mathbf{s}}_i = -\frac{\gamma}{m}\mathbf{s}_i - \mathbf{v}_j \cdot \nabla_i\nabla_j\frac{U_{tot}}{m} + \frac{\mathbf{F}_i}{m\tau} + \frac{\gamma v_0}{m}\sqrt{\frac{2}{\tau}}\boldsymbol{\eta}_i \times \hat{\mathbf{n}}_i + \frac{\gamma}{m}\mathbf{v}_i\left(v_0\frac{\beta}{\gamma_r} - \frac{1}{\tau}\right) - \frac{\gamma v_0}{m}\frac{\beta}{\gamma_r}\left[\left(\frac{\mathbf{v}_i}{v_0} - \frac{\mathbf{F}_i}{\gamma v_0}\right)\mathbf{v}_i \cdot \left(\frac{\mathbf{v}_i}{v_0} - \frac{\mathbf{F}_i}{\gamma v_0}\right)\right]. \tag{13}$$

By taking the overdamped limit $m/\gamma \to 0$, one can eliminate the variable $\mathbf{s}_i$, effectively neglecting the time evolution of the acceleration, i.e., $\dot{\mathbf{s}}_i = 0$. In this way, we obtain an equation of motion for $\mathbf{v}_i$, which reads

$$\mathbf{s}_i = \dot{\mathbf{v}}_i = -\mathbf{v}_j \cdot \nabla_i\nabla_j\frac{U_{tot}}{\gamma} + \frac{\mathbf{F}_i}{\gamma\tau} + v_0\sqrt{\frac{2}{\tau}}\boldsymbol{\eta}_i \times \hat{\mathbf{n}}_i + \mathbf{v}_i\left(v_0\frac{\beta}{\gamma_r} - \frac{1}{\tau}\right) - v_0\frac{\beta}{\gamma_r}\left[\left(\frac{\mathbf{v}_i}{v_0} - \frac{\mathbf{F}_i}{\gamma v_0}\right)\mathbf{v}_i \cdot \left(\frac{\mathbf{v}_i}{v_0} - \frac{\mathbf{F}_i}{\gamma v_0}\right)\right]. \tag{14}$$

The first term in Eq. (14) is a local alignment term. Indeed, by calling n_i the instantaneous number of particles interacting with the particle i, we have

$$\begin{aligned}\sum_j \nabla_i\nabla_j U_{tot} \cdot \mathbf{v}_j &= \sum_j \nabla_i\nabla_j \sum_{k<l} U(|\mathbf{x}_{kl}|) \cdot \mathbf{v}_j \\ &= \sum_{j=1}^{n_i} \nabla_i\nabla_i U(|\mathbf{x}_{ij}|) \cdot \mathbf{v}_i + \sum_{j=1}^{n_i} \nabla_i\nabla_j U(|\mathbf{x}_{ij}|) \cdot \mathbf{v}_j \\ &= \sum_{j=1}^{n_i} \nabla_i\nabla_i U \cdot (\mathbf{v}_i - \mathbf{v}_j),\end{aligned} \tag{15}$$

with $\mathbf{x}_{ij} = \mathbf{x}_j - \mathbf{x}_i$. We remark that Eq. (15) holds for a general total potential $U_{\text{tot}} = \sum_{i<j} U(|\mathbf{x}_{ij}|)$, i.e., a sum of pairwise contributions. In this interaction, the particle's velocity v_i is attracted to the velocity of particle j, depending on the second derivative of the potential via the term $\nabla_i\nabla_i U(|\mathbf{x}_{ij}|)$. The other terms in the first line of Eq. (14) are a force $\mathbf{F}_i$ normalized by the persistence time τ and a noise term. Finally, self-alignment induces other single-particle non-linear terms that depend on $\mathbf{v}_i$ and $\mathbf{F}_i$ [second line of Eq. (14), terms $\propto \beta$].

We remark that the dynamics (14) can be obtained directly by taking the overdamped limit of the equation of motion for the translational velocity, i.e., by assuming $\dot{\mathbf{v}}_i \approx 0$ in Eq. (9a), which is valid for small inertial times.

Lattice approximation

In a crystal configuration, the particles are placed on an ordered lattice, for instance, a triangular one in two dimensions, and display small fluctuations around their lattice positions. To proceed further, we consider the lattice approximation, effectively freezing the particle positions on their lattice sites. This assumption implies that the

net force on each particle vanishes, $\mathbf{F}_i = 0$. In addition, by considering a short-range potential U as the WCA potential used in the simulations, the second derivative of the potential becomes constant and can be expressed as

$$\sum_{j=1}^{n_i} \nabla_i \nabla_i U(|\mathbf{x}_{ij}|) \cdot (\mathbf{v}_i - \mathbf{v}_j) = \sum_{j=1}^{n_i} \boldsymbol{\mathcal{H}}_j \cdot (\mathbf{v}_i - \mathbf{v}_j), \tag{16}$$

where $n_i = 6$ selects the first neighbors of the particle i in a two-dimensional triangular lattice. The constant matrix $\boldsymbol{\mathcal{H}}_j$ (depending on the distance between the particle i and the particle j) can be obtained by calculating the second spatial derivatives of the potential $U = U(r_{ij})$,

$$\nabla_i^\alpha \nabla_i^\beta U = \left[U'' + \frac{U'}{|r_{ij}|} \right] \frac{r_{ij}^\alpha r_{ij}^\beta}{|r_{ij}|^2} - \delta_{\alpha\beta} \frac{U'}{|r_{ij}|}, \tag{17}$$

where $r_{ij}^\alpha = r_i^\alpha - r_j^\alpha$, with $\alpha = x, y$. In this expression, each prime on the potential U means a spatial derivative. In addition, the following relation holds:

$$\nabla_i^\alpha \nabla_j^\beta U = -\nabla_i^\alpha \nabla_i^\beta U. \tag{18}$$

The Cartesian components of $r_{ij}^\alpha / |r_{ij}|$ can be expressed as $\cos(\delta_j)$ and $\sin(\delta_j)$ after introducing the angle δ_j between the $\mathbf{r}_{ij}$ vector and the horizontal axis. The regular hexagonal structure of the cluster allows us to express the angle as $\delta_j = \delta_0 + j\pi/3$, where $j = 0, 1, \ldots, 5$, and δ_0 is the orientation of the hexagon with respect to the reference frame that we fix to zero without loss of generality. In this way, we finally obtain the elements of the matrix $\boldsymbol{\mathcal{H}}$, which have the following form:

$$\mathcal{H}_{xx}(\sigma) = U''(\sigma) \cos^2\left(j\frac{\pi}{3}\right) + \frac{U'(\sigma)}{\sigma} \sin^2\left(j\frac{\pi}{3}\right), \tag{19}$$

$$\mathcal{H}_{yy}(\sigma) = U''(\sigma) \sin^2\left(j\frac{\pi}{3}\right) + \frac{U'(\sigma)}{\sigma} \cos^2\left(j\frac{\pi}{3}\right), \tag{20}$$

$$\mathcal{H}_{xy}(\sigma) = \left(U''(\sigma) - \frac{U'(\sigma)}{\sigma} \right) \cos\left(j\frac{\pi}{3}\right) \sin\left(j\frac{\pi}{3}\right), \tag{21}$$

with $\mathcal{H}_{xy}(\sigma) = \mathcal{H}_{yx}(\sigma)$. Here, we have suppressed the explicit dependence on j. Finally, we remark that the sum over the six neighbors of the out-of-diagonal elements of $\boldsymbol{\mathcal{H}}$ vanishes,

$$\sum_{j=1}^{n_i} \mathcal{H}_{xy}(\sigma) = 0. \tag{22}$$

The same protocol applied to the diagonal elements gives a constant $\mathcal{K} \neq 0$ with the following expression:

$$\mathcal{K} = \sum_{j=1}^{n_i} \mathcal{H}_{xx}(\sigma) = 3\left(U''(\sigma) + \frac{U'(\sigma)}{\sigma} \right), \tag{23}$$

with $\sum_{j=1}^{n_i} \mathcal{H}_{xx}(\sigma) = \sum_{j=1}^{n_i} \mathcal{H}_{yy}(\sigma)$. In this way, we have

$$\sum_{j=1}^{n_i} \boldsymbol{\mathcal{H}}_j = \mathcal{K}\boldsymbol{\mathcal{I}}, \tag{24}$$

where $\boldsymbol{\mathcal{I}}$ is the identity matrix. We remark that truncating at first neighbors to estimate the second derivative of the potential works because the potential is short-range, as in the simulations of the main text.

By summarizing, the particle dynamics in the lattice approximation can be expressed as

$$\dot{\mathbf{v}}_i = \mathbf{s}_i = -\frac{1}{\gamma} \sum_{j=1}^{n_i} \mathcal{K}(\mathbf{v}_i - \mathbf{v}_j) - \mathbf{v}_i \left(\frac{1}{\tau} - \frac{\beta}{\gamma_r} v_0 \right) - \frac{\beta}{v_0 \gamma_r} \mathbf{v}_i |\mathbf{v}_i|^2 + v_0 \sqrt{\frac{2}{\tau}} \boldsymbol{\eta}_i \times \hat{\mathbf{n}}_i, \tag{25}$$

where the constant $\mathcal{K}$ is defined by Eq. (23) and we have neglected the directional contribution of the lattice. In this way, the first term on the right-hand side of Eq. (25) (first line) corresponds to a discrete Laplacian. By keeping directional contribution, the only change regards the inclusion of directional contribution, accounting for the lattice orientation. Finally, the dynamics (12) can be expressed as the functional derivative of a free-energy functional,

$$\dot{\mathbf{v}}_i = -\frac{1}{\tau} \frac{\delta}{\delta \mathbf{v}_i} \mathcal{F}[\{\mathbf{v}\}] + v_0 \sqrt{\frac{2}{\tau}} \boldsymbol{\eta}_i \times \hat{\mathbf{n}}_i, \tag{26}$$

where $\mathcal{F}[\{\mathbf{v}\}]$ is defined as

$$\mathcal{F}[\{\mathbf{v}\}] = \frac{\tau \mathcal{K}}{2\gamma} \sum_{i<j} \mathbf{v}_j \cdot \mathbf{v}_i + \frac{1}{4} \sum_i \frac{\beta}{\gamma_r v_0} |\mathbf{v}_i|^4 + \frac{1}{2} \sum_i |\mathbf{v}_i|^2 \left(1 - v_0 \frac{\tau\beta}{\gamma_r} \right). \tag{27}$$

Structural analysis

In this section, we demonstrate that our system—self-aligning active particles at packing fraction $\Phi = 1.1$—is characterized by an almost perfect hexagonal order, i.e., it displays a crystalline structure independently of the self-alignment strength. Although the aspect ratio $\sqrt{3}/2$ required for such a structure is not satisfied in our system, the crystal, nevertheless, emerges due to periodic boundary conditions and a sufficiently large system size, as illustrated by the local snapshots [see Figs. 6(a) and 6(b) for the disordered and flocking phases, respectively]. In addition, we analyze the orientational order parameter,

$$\psi_6^j = \frac{1}{n_j} \sum_{l=1}^{n_j} \exp\left[i 6 \theta_{lj} \right], \tag{28}$$

where n_j denotes the total number of neighbors of the j-th particle. The term θ_{lj} denotes the angle between the vector $\mathbf{x}_{lj} = \mathbf{x}_j - \mathbf{x}_l$ and the horizontal (x) direction. To quantitatively analyze the degree of order in the system, we plot the average value of the orientational order parameter $\psi_6 = 1/N \sum_{j=1}^{N} \langle \psi_6^j \rangle$, averaged in the steady-state over all particles and over time, as a function of system size. This observable approaches unity for a crystalline structure and is close to zero for a liquid-like structure. As shown in Fig. 6(c), the observable $1 - \psi_6$ approaches a value near zero for sufficiently large system sizes, both in the disordered and ordered phases, indicating an almost perfect hexagonal structure. The two almost coinciding open circles in Fig. 6(c) represent the same observable computed for a simulation box with aspect ratio $\sqrt{3}/2$, where the horizontal axis

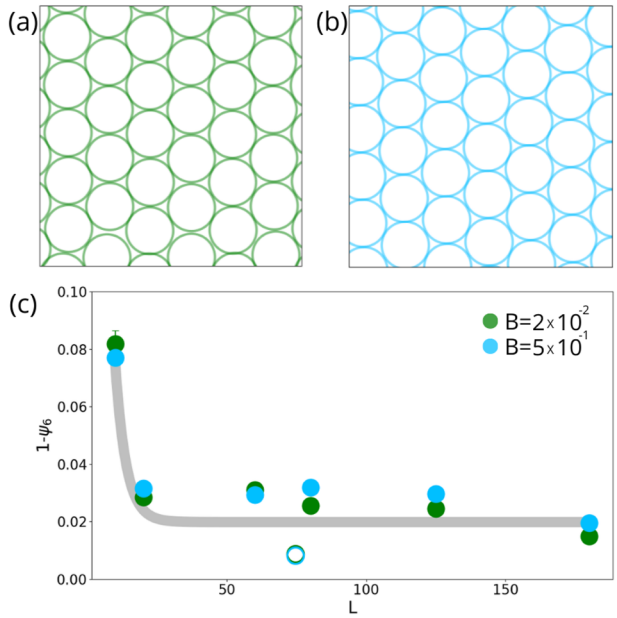

FIG. 6. Hexagonal lattice order. Snapshots showing the hexagonal lattice structure obtained for (a) $B = 0.02$ (disordered phase) and (b) $B = 0.5$ (flocking phase). (c) Behavior of $1 - \psi_6$ as a function of the system size: green dots correspond to $B = 0.02$ (disordered phase), while blue dots correspond to $B = 0.5$ (flocking phase). The local hexagonal order parameter $\psi_6^j = 1/n_j \sum_{l=1}^{n_j} \exp[i6\theta_{lj}]$ is averaged over all particles in the system and over time after reaching the steady-state $\psi_6 = 1/N \sum_{j=1}^{N} \langle \psi_6^j \rangle$. The two almost coinciding open circles (green for $B = 0.02$ and blue for $B = 0.5$) represent simulations performed in a rectangular box with aspect ratio $\sqrt{3}/2$, where the horizontal coordinate corresponds to $\sqrt{L_x L_y}$, for $B = 0.02$ and $B = 0.5$. The gray line is a guide for the eye.

is defined as $\sqrt{L_x L_y}$. These values are slightly smaller than those obtained using square boxes, but they remain consistent with the previous results, further confirming the high degree of hexagonal ordering achieved. In other words, the defects introduced by using a square box are negligible.

Continuum limit

Here, we consider the continuum limit by replacing $\mathbf{v}_i \to \mathbf{v}(\mathbf{r})$, where $\mathbf{r}$ is a continuous coordinate on the lattice. In this way, the discrete Laplacian in Eq. (25) (the first term in the right-hand-side) is replaced by

$$-\frac{1}{\gamma}\sum_{j=1}^{n_i} \mathcal{K}(\mathbf{v}_i - \mathbf{v}_j) \to \frac{3\sigma^2}{2}\frac{\mathcal{K}}{\gamma}\nabla^2\mathbf{v}(\mathbf{r}), \tag{29}$$

where the particle diameter σ also corresponds to the lattice constant. The dynamics (12) in the continuum limit becomes a dynamics for the velocity field $\mathbf{v}(\mathbf{r})$,

$$\dot{\mathbf{v}}(\mathbf{r},t) = -\frac{1}{\tau}\frac{\delta}{\delta \mathbf{v}(\mathbf{r},t)}\mathcal{F}[\mathbf{v}(\mathbf{r},t)] + v_0\sqrt{\frac{2}{\tau}}\boldsymbol{\eta}(\mathbf{r},t). \tag{30}$$

Here, we approximate the noise projection in Eq. (26) by a vector of independent white noises, $\boldsymbol{\eta}(\mathbf{r},t)$, such that $\langle \boldsymbol{\eta}(\mathbf{r},t)\boldsymbol{\eta}(\mathbf{r}',t')\rangle = \delta(t-t')\delta(\mathbf{r}-\mathbf{r}')$. This corresponds to replacing the active Brownian particle dynamics with its active Ornstein–Uhlenbeck approximation, which—as shown in Ref. 77—preserves the first and second moments of the stationary distribution. In addition, $\mathcal{F}[\mathbf{v}(\mathbf{r},t)]$ is the Landau–Ginzburg free energy, which reads

$$\mathcal{F}[\mathbf{v}(\mathbf{r},t)] = \int d\mathbf{r}\frac{3\tau\sigma^2}{2}\frac{\mathcal{K}}{\gamma}(\nabla v(\mathbf{r},t))^2 + \int d\mathbf{r}\frac{|\mathbf{v}(\mathbf{r},t)|^2}{2}\left(1 - v_0\frac{\tau\beta}{\gamma_r}\right) + \int d\mathbf{r}\frac{\tau\beta}{4v_0\gamma_r}|\mathbf{v}(\mathbf{r},t)|^4. \tag{31}$$

The first term on the right-hand-side of Eq. (31) (first line) corresponds to a kinetic term that restores random configurations, while the other two terms coincide with a single-particle free-energy with a Mexican hat shape depending on the sign of the mass term. As a consequence, the flocking transition occurs for

$$\frac{\beta}{\gamma_r} > \frac{\beta_c}{\gamma_r} = \frac{1}{\tau v_0}, \tag{32}$$

where the quadratic term changes sign and the typical length of the self-alignment mechanism is equal to the persistence length.

Prediction for the polarization

To predict the polarization value before and after the flocking transition, we calculate the average velocity predicted by the Landau–Ginzburg model, theoretically linked to the dynamics of a self-aligning active crystal. In particular, before the flocking transition $\beta < \beta_c$ $(B < B_c)$, the average velocity is zero, and any residual velocity is due to finite size effects. By contrast, in the flocking phase, $\beta > \beta_c$ $(B > B_c)$, the average velocity is different from zero and directed along $\hat{\mathbf{n}}$, which corresponds to the average direction of the flock. Summarizing, the average velocity $\langle \mathbf{v} \rangle$ has the following expression:

$$\langle \mathbf{v} \rangle = \begin{cases} 0, & \beta < \beta_c, \\ \left(\frac{v_0}{\beta}\right)^{1/2}\left(v_0\frac{\beta}{\gamma_r} - \frac{1}{\tau}\right)^{1/2}\hat{\mathbf{n}}, & \beta > \beta_c, \end{cases} \tag{33}$$

where the amplitude of $\langle \mathbf{v} \rangle$ is obtained by calculating the minima of the velocity-dependent Landau–Ginzburg free energy. As a result, we can estimate the polarization as

$$\mathbf{S} = \frac{\langle \mathbf{v} \rangle}{|\mathbf{v}|} \approx \frac{\langle \mathbf{v} \rangle}{v_0}. \tag{34}$$

The polarization $\mathbf{S}$ is zero before the flocking transition point, while it is given by the following expression:

$$|\mathbf{S}| \approx \left(\frac{\gamma_r}{\beta}\right)^{1/2}\left(\frac{\beta}{\gamma_r} - \frac{1}{v_0\tau}\right)^{1/2} \propto \frac{\sqrt{B - B_c}}{\sqrt{B}}, \tag{35}$$

after the transition. The polarization tends to 1 for $v_0\beta/\gamma_r \gg 1/\tau$, as expected. To compare this profile with simulations, we have included an additive constant to the profile (35). This constant accounts for the finite size effects of the system, which does not allow the polarization to exactly reach zero before the flocking transition.

Prediction for the spatial velocity correlations before the flocking transition

For a Landau–Ginzburg model, it is possible to calculate the shape of the steady-state spatial velocity correlations. In particular, before the flocking transition, we can neglect the quartic term of the interactions and, thus, non-linear effects in the dynamics for $\mathbf{v} = \mathbf{v}(\mathbf{r}, t)$, obtaining

$$\dot{\mathbf{v}} = \left(3\sigma^2 \mathcal{K}\nabla^2 - \left(\frac{1}{\tau} - v_0\frac{\beta}{\gamma_r}\right)\right)\mathbf{v} + v_0\sqrt{\frac{2}{\tau}}\boldsymbol{\eta}, \tag{36}$$

where $\boldsymbol{\eta} = \boldsymbol{\eta}(\mathbf{r}, t)$. By multiplying the equation by $\mathbf{v}(\mathbf{r}', t)$, we can obtain the equation for the spatial velocity correlations $C(\mathbf{r} - \mathbf{r}') = \langle \mathbf{v}(\mathbf{r}) \cdot \mathbf{v}(\mathbf{r}') \rangle$, which uniquely depends on the distance $\mathbf{r} - \mathbf{r}'$,

$$\frac{\partial}{\partial t} C(\mathbf{r} - \mathbf{r}') = \left(3\sigma^2 \mathcal{K}\nabla^2 - \left(\frac{1}{\tau} - v_0\frac{\beta}{\gamma_r}\right)\right) C(\mathbf{r} - \mathbf{r}') + 2\frac{v_0^2}{\tau}\delta(\mathbf{r} - \mathbf{r}'), \tag{37}$$

where we have used the Novikov theorem to calculate the velocity-noise correlation $\langle \mathbf{v}(\mathbf{r}', t)\boldsymbol{\eta}(\mathbf{r}, t) \rangle = v_0\sqrt{\frac{2}{\tau}}\delta(\mathbf{r} - \mathbf{r}')$. By taking the steady-state solution (neglecting $\partial_t C = 0$), we obtain a Helmholtz equation in two dimensions with the solution

$$C(\mathbf{r}) = \frac{v_0^2}{3\pi\tau\sigma^2\mathcal{K}} K_0\left(\frac{|\mathbf{r}|}{\xi}\right). \tag{38}$$

Here, K_0 is the Bessel function of the second kind, and ξ is a correlation length, which is given by

$$\xi = \frac{\sigma\sqrt{3\tau\mathcal{K}}}{\left(1 - \frac{v_0\tau\beta}{\gamma_r}\right)^{1/2}}, \tag{39}$$

which corresponds to the prediction (7) of the main text. Finally, we can approximate the Bessel function for long distances $|\mathbf{r}| > \xi$, obtaining

$$C(r) \sim \sqrt{\frac{\xi}{r}} \exp\left\{\left(-\frac{r}{\xi}\right)\right\}, \tag{40}$$

where $r = |\mathbf{r}|$. This expression corresponds to the prediction of the main text, which is compared with numerical data.

Theory for a different self-aligning mechanism

Our theory can be easily adapted to other self-aligning mechanisms, which would qualitatively lead to similar flocking behavior. However, adopting a different self-alignment rule could produce a velocity-dependent free energy with a different functional form.

As an example, we now consider a different self-alignment mechanism in the dynamics of the particle orientation [Eqs. (9a) and (9b)],

$$\tilde{\beta}\left(\hat{\mathbf{n}}_i \times \frac{\mathbf{v}_i}{|\mathbf{v}_i|}\right) \times \hat{\mathbf{n}}_i = \tilde{\beta}\left(\frac{\mathbf{v}_i}{|\mathbf{v}_i|} - \hat{\mathbf{n}}_i\left[\frac{\mathbf{v}_i}{|\mathbf{v}_i|} \cdot \hat{\mathbf{n}}_i\right]\right). \tag{41}$$

This mechanism is often employed in numerical studies of cells.[40,41] Here, $\tilde{\beta}$ can be interpreted as the self-alignment strength. By repeating the calculations presented in the section "Derivation of the theoretical results," starting from Eq. (11), we obtain a dynamics equivalent to Eq. (25), valid under the same approximations,

$$\dot{\mathbf{v}}_i = -\frac{1}{\gamma}\sum_{j=1}^{n_i} \mathcal{K}(\mathbf{v}_i - \mathbf{v}_j) - \mathbf{v}_i\left(\frac{1}{\tau}\right) \tag{42}$$

$$+ \frac{\tilde{\beta}}{\gamma_r} v_0 \frac{\mathbf{v}_i}{|\mathbf{v}_i|} - \frac{\tilde{\beta}}{v_0\gamma_r}\mathbf{v}_i|\mathbf{v}_i| + v_0\sqrt{\frac{2}{\tau}}\boldsymbol{\eta}_i \times \hat{\mathbf{n}}_i. \tag{43}$$

This equation of motion can be rewritten as

$$\dot{\mathbf{v}}_i = -\frac{1}{\tau}\frac{\delta}{\delta\mathbf{v}_i}\tilde{\mathcal{F}}[\{\mathbf{v}\}] + v_0\sqrt{\frac{2}{\tau}}\boldsymbol{\eta}_i \times \hat{\mathbf{n}}_i \tag{44}$$

in terms of an effective velocity-dependent free energy with the following shape:

$$\tilde{\mathcal{F}}[\{\mathbf{v}\}] = \frac{\tau\mathcal{K}}{2\gamma}\sum_{i<j}\mathbf{v}_j \cdot \mathbf{v}_i + \frac{1}{3}\sum_i \frac{\tilde{\beta}}{\gamma_r v_0}|\mathbf{v}_i|^3 + \frac{1}{2}\sum_i |\mathbf{v}_i|^2 - v_0\frac{\tau\tilde{\beta}}{\gamma_r}\sum_i |\mathbf{v}_i|. \tag{45}$$

Even though $\tilde{\mathcal{F}}[\mathbf{v}]$ does not have the standard Landau–Ginzburg form, it can still reproduce flocking behavior for parameter values where the free energy minimum is far from the origin.

ACKNOWLEDGMENTS

H.L. acknowledges the support from the Deutsche Forschungsgemeinschaft (DFG) through the SPP 2265 under Grant No. LO 418/25. L.C. acknowledges financial support from the University of Rome Sapienza under the project Ateneo 2024 (Grant No. RM124190C54BE48D), "Elementary excitations at the origin of glassy or hexatic behavior in low dimensional system, at and out of equilibrium."

AUTHOR DECLARATIONS

Conflict of Interest

The authors have no conflicts to disclose.

Author Contributions

Marco Musacchio: Conceptualization (equal); Data curation (lead); Formal analysis (lead); Investigation (lead); Methodology (lead); Software (lead); Writing – original draft (equal); Writing – review & editing (equal). **Alexander P. Antonov**: Investigation (equal); Supervision (equal); Validation (equal); Writing – original draft (equal); Writing – review & editing (equal). **Hartmut Löwen**: Funding acquisition (equal); Investigation (equal); Project administration (equal); Supervision (equal); Validation (equal); Writing – original draft (equal); Writing – review & editing (equal). **Lorenzo Caprini**: Conceptualization (equal); Funding acquisition (equal); Supervision (lead); Validation (lead); Writing – original draft (equal); Writing – review & editing (equal).

DATA AVAILABILITY

The data that support the plots within this paper and other findings of this study are available from the corresponding author upon request.

REFERENCES

[1] M. C. Marchetti, J. F. Joanny, S. Ramaswamy, T. B. Liverpool, J. Prost, M. Rao, and R. A. Simha, Rev. Mod. Phys. **85**, 1143 (2013).
[2] J. Elgeti, R. G. Winkler, and G. Gompper, Rep. Prog. Phys. **78**, 056601 (2015).
[3] D. B. Kearns, Nat. Rev. Microbiol. **8**, 634 (2010).
[4] R. Alert and X. Trepat, Annu. Rev. Condens. Matter Phys. **11**, 77 (2020).
[5] C. Bechinger, R. Di Leonardo, H. Löwen, C. Reichhardt, G. Volpe, and G. Volpe, Rev. Mod. Phys. **88**, 045006 (2016).
[6] A. Bricard, J.-B. Caussin, N. Desreumaux, O. Dauchot, and D. Bartolo, Nature **503**, 95 (2013).
[7] D. Geyer, D. Martin, J. Tailleur, and D. Bartolo, Phys. Rev. X **9**, 031043 (2019).
[8] A. E. Turgut, H. Çelikkanat, F. Gökçe, and E. Şahin, Swarm Intell. **2**, 97 (2008).
[9] G. Vásárhelyi, C. Virágh, G. Somorjai, T. Nepusz, A. E. Eiben, and T. Vicsek, Sci. Robot. **3**, eaat3536 (2018).
[10] M. Agrawal and S. C. Glotzer, Proc. Natl. Acad. Sci. U. S. A. **117**, 8700 (2020).
[11] J. Deseigne, O. Dauchot, and H. Chaté, Phys. Rev. Lett. **105**, 098001 (2010).
[12] N. Kumar, H. Soni, S. Ramaswamy, and A. K. Sood, Nat. Commun. **5**, 4688 (2014).
[13] C. Virágh, G. Vásárhelyi, N. Tarcai, T. Szörényi, G. Somorjai, T. Nepusz, and T. Vicsek, Bioinspir. Biomim. **9**, 025012 (2014).
[14] L. Chen, K. J. Welch, P. Leishangthem, D. Ghosh, B. Zhang, T.-P. Sun, J. Klukas, Z. Tu, X. Cheng, and X. Xu, arXiv:2302.10525 (2023).
[15] S. Das, M. Ciarchi, Z. Zhou, J. Yan, J. Zhang, and R. Alert, Phys. Rev. X **14**, 031008 (2024).
[16] M. Brambilla, E. Ferrante, M. Birattari, and M. Dorigo, Swarm Intell. **7**, 1 (2013).
[17] T. Vicsek and A. Zafeiris, Phys. Rep. **517**, 71 (2012).
[18] P. Romanczuk, M. Bär, W. Ebeling, B. Lindner, and L. Schimansky-Geier, Eur. Phys. J. Spec. Top. **202**, 1 (2012).
[19] A. P. Solon and J. Tailleur, Phys. Rev. Lett. **111**, 078101 (2013).
[20] L. Barberis and F. Peruani, Phys. Rev. Lett. **117**, 248001 (2016).
[21] S. Shankar, M. J. Bowick, and M. C. Marchetti, Phys. Rev. X **7**, 031039 (2017).
[22] M. Casiulis, M. Tarzia, L. F. Cugliandolo, and O. Dauchot, Phys. Rev. Lett. **124**, 198001 (2020).
[23] D. Geiß, K. Kroy, and V. Holubec, Phys. Rev. E **106**, 014609 (2022).
[24] J. J. Binney, N. J. Dowrick, A. J. Fisher, and M. E. Newman, *The Theory of Critical Phenomena: An Introduction to the Renormalization Group* (Oxford University Press, 1992).
[25] A. Cavagna and I. Giardina, Annu. Rev. Condens. Matter Phys. **5**, 183 (2014).
[26] A. Cavagna, D. Conti, C. Creato, L. Del Castello, I. Giardina, T. S. Grigera, S. Melillo, L. Parisi, and M. Viale, Nat. Phys. **13**, 914 (2017).
[27] T. Ihle, Phys. Rev. E **83**, 030901 (2011).
[28] R. Lier, Phys. Rev. E **113**, 044116 (2026).
[29] R. Kürsten and T. Ihle, Phys. Rev. E **104**, 034604 (2021).
[30] J. Toner, Y. Tu, and S. Ramaswamy, Ann. Phys. **318**, 170 (2005).
[31] E. Bertin, M. Droz, and G. Grégoire, Phys. Rev. E **74**, 022101 (2006).
[32] F. D. C. Farrell, M. C. Marchetti, D. Marenduzzo, and J. Tailleur, Phys. Rev. Lett. **108**, 248101 (2012).
[33] A. Peshkov, I. S. Aranson, E. Bertin, H. Chaté, and F. Ginelli, Phys. Rev. Lett. **109**, 268701 (2012).
[34] R. Chatterjee, N. Rana, R. A. Simha, P. Perlekar, and S. Ramaswamy, Phys. Rev. X **11**, 031063 (2021).
[35] P. Baconnier, O. Dauchot, V. Démery, G. Düring, S. Henkes, C. Huepe, and A. Shee, Rev. Mod. Phys. **97**, 015007 (2025).
[36] H. Chaté, F. Ginelli, G. Grégoire, F. Peruani, and F. Raynaud, Eur. Phys. J. B **64**, 451 (2008).
[37] D. Levis, I. Pagonabarraga, and B. Liebchen, Phys. Rev. Res. **1**, 023026 (2019).
[38] K. L. Kreienkamp and S. H. L. Klapp, New J. Phys. **24**, 123009 (2022).
[39] J. Giraldo-Barreto and V. Holubec, Phys. Rev. E **112**, L032103 (2025).
[40] B. Szabo, G. Szöllösi, B. Gönci, Z. Jurányi, D. Selmeczi, and T. Vicsek, Phys. Rev. E **74**, 061908 (2006).
[41] C. Malinverno, S. Corallino, F. Giavazzi, M. Bergert, Q. Li, M. Leoni, A. Disanza, E. Frittoli, A. Oldani, E. Martini *et al.*, Nat. Mater. **16**, 587 (2017).
[42] D. L. Barton, S. Henkes, C. J. Weijer, and R. Sknepnek, PLoS Comput. Biol. **13**, e1005569 (2017).
[43] F. Giavazzi, M. Paoluzzi, M. Macchi, D. Bi, G. Scita, M. L. Manning, R. Cerbino, and M. C. Marchetti, Soft Matter **14**, 3471 (2018).
[44] Y. Shen, J. O'Byrne, A. Schoenit, A. Maitra, R.-M. Mège, R. Voituriez, and B. Ladoux, Proc. Natl. Acad. Sci. U. S. A. **122**, e2421327122 (2025).
[45] O. Dauchot and V. Démery, Phys. Rev. Lett. **122**, 068002 (2019).
[46] F. Siebers, A. Jayaram, P. Blümler, and T. Speck, Sci. Adv. **9**, eadf5443 (2023).
[47] L. Caprini, D. Breoni, A. Ldov, C. Scholz, and H. Löwen, Commun. Phys. **7**, 343 (2024).
[48] L. Giomi, N. Hawley-Weld, and L. Mahadevan, Proc. R. Soc. A **469**, 20120637 (2013).
[49] A. Deblais, T. Barois, T. Guerin, P.-H. Delville, R. Vaudaine, J. S. Lintuvuori, J.-F. Boudet, J.-C. Baret, and H. Kellay, Phys. Rev. Lett. **120**, 188002 (2018).
[50] M. Leoni, M. Paoluzzi, S. Eldeen, A. Estrada, L. Nguyen, M. Alexandrescu, K. Sherb, and W. W. Ahmed, Phys. Rev. Res. **2**, 043299 (2020).
[51] C. Tapia-Ignacio, L. L. Gutierrez-Martinez, and M. Sandoval, J. Stat. Mech.: Theory Exp. **2021**, 053404.
[52] A. Altshuler, O. L. Bonomo, N. Gorohovsky, S. Marchini, E. Rosen, O. Tal-Friedman, S. Reuveni, and Y. Roichman, Phys. Rev. Res. **6**, 023255 (2024).
[53] I. S. Aranson, D. Volfson, and L. S. Tsimring, Phys. Rev. E **75**, 051301 (2007).
[54] A. Kudrolli, G. Lumay, D. Volfson, and L. S. Tsimring, Phys. Rev. Lett. **100**, 058001 (2008).
[55] N. Koumakis, A. Gnoli, C. Maggi, A. Puglisi, and R. Di Leonardo, New J. Phys. **18**, 113046 (2016).
[56] C. Scholz, M. Engel, and T. Pöschel, Nat. Commun. **9**, 931 (2018).
[57] M. A. López-Castaño, A. M. Seco, A. M. Seco, Á. Rodríguez-Rivas, and F. V. Reyes, Phys. Rev. Res. **4**, 033230 (2022).
[58] A. P. Antonov, L. Caprini, A. Ldov, C. Scholz, and H. Löwen, Phys. Rev. Lett. **133**, 198301 (2024).
[59] A. P. Antonov, M. Musacchio, H. Löwen, and L. Caprini, Nat. Commun. **16**, 7235 (2025).
[60] K.-D. N. T. Lam, M. Schindler, and O. Dauchot, New J. Phys. **17**, 113056 (2015).
[61] M. Casiulis, E. Arbel, C. van Waes, Y. Lahini, S. Martiniani, N. Oppenheimer, and M. Y. B. Zion, Proc. Natl. Acad. Sci. U. S. A. **122**, e2502211122 (2025).
[62] N. Shimoyama, K. Sugawara, T. Mizuguchi, Y. Hayakawa, and M. Sano, Phys. Rev. Lett. **76**, 3870 (1996).
[63] S. Henkes, Y. Fily, and M. C. Marchetti, Phys. Rev. E **84**, 040301 (2011).
[64] D. Canavello, R. H. Damascena, L. R. E. Cabral, and C. C. de Souza Silva, Soft Matter **20**, 2310 (2024).
[65] M. Musacchio, A. P. Antonov, H. Löwen, and L. Caprini, J. Chem. Phys. **162**, 244902 (2025).
[66] M. Paoluzzi, D. Levis, and I. Pagonabarraga, Commun. Phys. **7**, 57 (2024).
[67] E. Ferrante, A. E. Turgut, M. Dorigo, and C. Huepe, Phys. Rev. Lett. **111**, 268302 (2013).
[68] E. Ferrante, A. E. Turgut, M. Dorigo, and C. Huepe, New J. Phys. **15**, 095011 (2013).
[69] P. Baconnier, D. Shohat, C. H. López, C. Coulais, V. Démery, G. Düring, and O. Dauchot, Nat. Phys. **18**, 1234 (2022).
[70] Y. Kinoshita, N. Uchida, and A. M. Menzel, J. Chem. Phys. **162**, 054906 (2025).
[71] U. M. B. Marconi and C. Maggi, Soft Matter **11**, 8768 (2015).
[72] É. Fodor, C. Nardini, M. E. Cates, J. Tailleur, P. Visco, and F. van Wijland, Phys. Rev. Lett. **117**, 038103 (2016).
[73] C. Maggi, U. M. B. Marconi, N. Gnan, and R. Di Leonardo, Sci. Rep. **5**, 10742 (2015).
[74] S. Das, G. Gompper, and R. G. Winkler, New J. Phys. **20**, 015001 (2018).
[75] U. M. B. Marconi, N. Gnan, M. Paoluzzi, C. Maggi, and R. Di Leonardo, Sci. Rep. **6**, 23297 (2016).

[76]L. Caprini, U. Marini Bettolo Marconi, and A. Puglisi, Phys. Rev. Lett. **124**, 078001 (2020).
[77]L. Caprini, A. R. Sprenger, H. Löwen, and R. Wittmann, J. Chem. Phys. **156**, 071102 (2022).
[78]L. Caprini, U. M. B. Marconi, C. Maggi, M. Paoluzzi, and A. Puglisi, Phys. Rev. Res. **2**, 023321 (2020).
[79]V. Berezinskii, Sov. Phys. JETP **32**, 493–500 (1971), [Zh. Eksp. Teor. Fiz. **3**, 907–920 (1971)].
[80]J. M. Kosterlitz and D. J. Thouless, J. Phys. C: Solid State Phys. **6**, 1181 (1973).
[81]J. M. Kosterlitz, J. Phys. C: Solid State Phys. **7**, 1046 (1974).
[82]J. M. Kosterlitz, Rep. Prog. Phys. **79**, 026001 (2016).
[83]A. Cavagna, I. Giardina, and T. S. Grigera, Phys. Rep. **728**, 1 (2018).
[84]K. Binder and D. Heermann, *Monte Carlo Simulation in Statistical Physics* (Springer, 1992), Vol. 8.
[85]L. Hostetler, R. Sakai, J. Zhang, A. Bazavov, and Y. Meurice, Phys. Rev. D **109**, 054514 (2024).
[86]D. R. Nelson and J. M. Kosterlitz, Phys. Rev. Lett. **39**, 1201 (1977).
[87]A. Shee, S. Henkes, and C. Huepe, Soft Matter **20**, 7865 (2024).
[88]U. M. B. Marconi and L. Caprini, Soft Matter **21**, 2586 (2025).
[89]S. Henkes, K. Kostanjevec, J. M. Collinson, R. Sknepnek, and E. Bertin, Nat. Commun. **11**, 1405 (2020).
[90]M. Musacchio, A. P. Antonov, H. Löwen, and L. Caprini, Soft Matter **22**, 2052 (2026).
[91]G. Baglietto and E. V. Albano, Phys. Rev. E **80**, 050103 (2009).
[92]M. Aldana, V. Dossetti, C. Huepe, V. M. Kenkre, and H. Larralde, Phys. Rev. Lett. **98**, 095702 (2007).
[93]H. Chaté, F. Ginelli, and G. Grégoire, Phys. Rev. Lett. **99**, 229601 (2007).
[94]J. Bialké, T. Speck, and H. Löwen, Phys. Rev. Lett. **108**, 168301 (2012).
[95]P. Digregorio, D. Levis, A. Suma, L. F. Cugliandolo, G. Gonnella, and I. Pagonabarraga, Phys. Rev. Lett. **121**, 098003 (2018).
[96]L. Caprini, U. Marini Bettolo Marconi, A. Puglisi, and H. Löwen, J. Chem. Phys. **159**, 041102 (2023).
[97]Y.-E. Keta, J. U. Klamser, R. L. Jack, and L. Berthier, Phys. Rev. Lett. **132**, 218301 (2024).
[98]L. Caprini and H. Löwen, Phys. Rev. Lett. **130**, 148202 (2023).
[99]R. Vyas, M. Casiulis, E. Arbel, C. van Waes, Y. Lahini, S. Martiniani, N. Oppenheimer, and M. Y. Ben Zion, Nat. Phys. **19**, 1235 (2023).
[100]C. Sándor, A. Libál, C. Reichhardt, and C. J. Olson Reichhardt, Phys. Rev. E **95**, 032606 (2017).
[101]P. Rahmani, F. Peruani, and P. Romanczuk, Commun. Phys. **4**, 206 (2021).
[102]M. Mangeat, S. Chatterjee, J. D. Noh, and H. Rieger, Commun. Phys. **8**, 186 (2025).
[103]E. Lång, A. Połeć, A. Lång, M. Valk, P. Blicher, A. D. Rowe, K. A. Tønseth, C. J. Jackson, T. P. Utheim, L. M. Janssen *et al.*, Nat. Commun. **9**, 3665 (2018).
[104]E. Lång, A. Lång, P. Blicher, T. Rognes, P. G. Dommersnes, and S. O. Bøe, Sci. Adv. **10**, eadk4825 (2024).
[105]F. Gu, B. Guiselin, N. Bain, I. Zuriguel, and D. Bartolo, Nature **638**, 112 (2025).
[106]H. Risken, *The Fokker-Planck Equation* (Springer, 1988).